Supplementary information:

A Mixed-Spin Spin-Crossover Thiozolylimine $[Fe_4L_6]^{8+}$ Cage

Li Li,[a] Alexander R. Craze,[a**] Outi Mustonen,[b] Hikaru Zenno,[c] Jacob J. Whittaker,[d] Shinya Hayami,[c] Leonard F. Lindoy,[e] Christopher E. Marjo,[b] Jack K. Clegg,[d] Janice R. Aldrich-Wright,[a] and Feng Li[a*]**

a. School of Science and Health, Western Sydney University, Locked Bag 1797, Penrith, NSW, 2751, Australia.
b. Mark Wainwright Analytical Centre, University of New South Wales, Kensington, NSW, 2052, Australia.
c. Department of Chemistry, Graduate School of Science and Technology, Kumamoto University, 2-39-1 Kurokami, Chuo-ku, Japan.
d. School of Chemistry and Molecular Biosciences, The University of Queensland, Brisbane St Lucia, QLD 4072, Australia.
e. School of Chemistry, The University of Sydney, NSW 2006, Australia.
**equal contribution

* Corresponding author:

Dr Feng Li
School of Science and Health
Western Sydney University
Locked Bag 1797, Penrith NSW 2751, Australia
Tel: +61 2 9685 9987
Fax: +61 2 9685 9915
E-mail: feng.li@westernsydney.edu.au

Experimental

Materials and synthesis

All reagents and solvents were purchased from commercial sources. 4,4′-diaminobiphenyl was prepared by adaptation of a literature procedure.[S1]

Physical measurements.

Elemental analysis was conducted at Macquarie university in the Chemical Analysis Facility. High resolution ESI-MS data were acquired using a Waters Xevo QToF mass spectrometer, operating in positive ion mode. FT-IR spectra were recorded on a Bruker Tensor 27 Fourier transform infrared spectrometer using diamond single bounce ATR sampling device. The UV-vis spectra were measured at ambient temperature using a Cary 100 spectrophotometer. Scanning electron microscopy was carried out on a PHENOM XL instrument using a CeB6 filament and a silicon drift EDX detector, with the accelerating voltage at 15 kV and the detector in backscatter mode. Magnetic susceptibility data were collected using a Quantum Design SQUID magnetometer calibrated against a standard palladium sample. The data were collected between 5 and 400 K and the scan rate of the temperature was fixed at 2.0 K min^{-1}. Measurements were taken continuously under an applied field of 0.5 T. X-ray photoelectron spectroscopy (XPS) was performed on an ESCALAB250Xi (Thermo Scientific, UK) intrument using a monochromated Al K alpha line (energy 1486.68 eV) at 150W (13 kV x 12 mA) with a spot size of 500 micrometre on the sample. Electron optics were arranged at 90 degrees with respect to the surface plane. Survey scans were performed with a pass energy of 100 eV with high-resolution scans performed at 20 eV. The complex was measured at 100 K, 125 K, 150 K, 175K, 200 K, 275 K, 310 K, 340 K, 400 K and then 500 K in the heating mode, and then remeasured at these temperatures in the cooling mode. Data was processed using the Avantage software package (Thermo Scientific, UK). Peaks were calibrated using the Fe2p3/2 peak at 706.9eV and background corrected using the Shirley method. TGA and DSC analysis were measured on a Netzsch STA449 Jupiter thermo-microbalance under an argon atmosphere, with a heating rate of 10 K per/min (sample used for such studies was dried under the vacuum).

L: 4,4′-Diaminobiphenyl (184 mg, 1.00 mmol) in ethanol (10 mL) was added to thiazole-4-carboxaldehyde (250 mg, 2.21 mmol) in ethanol (10 mL) leading to a clear yellow solution. The mixture was heated at reflux overnight with stirring and then the pale yellow precipitate was collected by filtration and washed with cold ethanol (3 x 5 mL) to give a yellow powder in 83% yield. This product was used directly in for complex synthesis without further purification.

The ligand proved difficult to dissolve in common organic solvents, including DMSO, therefore no NMR spectra were able to be obtained.

FT-IR (ATR, γ cm-1): 3038, 1620, 1593, 1494, 1425, 1210, 1147, 939, 887, 853, 830, 746, 722; UV–vis (solid state in nujol): λ_{max} 206 nm. ESI-HRMS (positive-ion detection, CH_3OH):

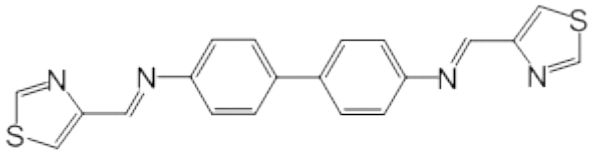

L

calculated for $[L + H]^+$, *m/z* = 375.0773; found 375.0738.

Figure S1. Structure of **L.**

$[Fe_4\mathbf{L}_6](BF_4)_8 \bullet 14H_2O \bullet 0.85CH_3CN$: Iron(II) tetrafluoroborate hexahydrate (30 mg, 0.09 mmol) in acetonitrile (5 mL) was slowly added to a suspension of **L** (50 mg, 0.13 mmol) in acetonitrile (10 mL). The reaction mixture starts to turn clear and the colour immediately changes to dark orange. After 4 hrs heating on 70 °C with stirring, the reaction solution was filtered and slow diffusion of diethyl ether into the filtrate resulted in the formation of dark red crystals of **1** suitable for single crystal X-ray diffraction analysis; these were subsequently air dried prior to elemental analysis. Yield, 61%. Elemental analysis (%) calcd for $C_{120}H_{84}B_8F_{32}Fe_4N_{24}S_{12}$ + $14H_2O$ + $0.85CH_3CN$: C42.35, H 3.35, N 10.08, S 11.15; found: C 42.57, H 3.01, N 9.76, S 10.81. FT-IR (ATR, cm^{-1}): 3113, 2349, 2323, 1587, 1487, 1051, 824, 671, 664; UV–vis (solid state in nujol): λ_{max} 520 nm; ESI-HRMS (positive-ion detection, CH_3CN): calculated for $[Fe_4\mathbf{L}_6 + (BF_4)]^{7+}$, *m/z* = 365.1626; found 365.1598.

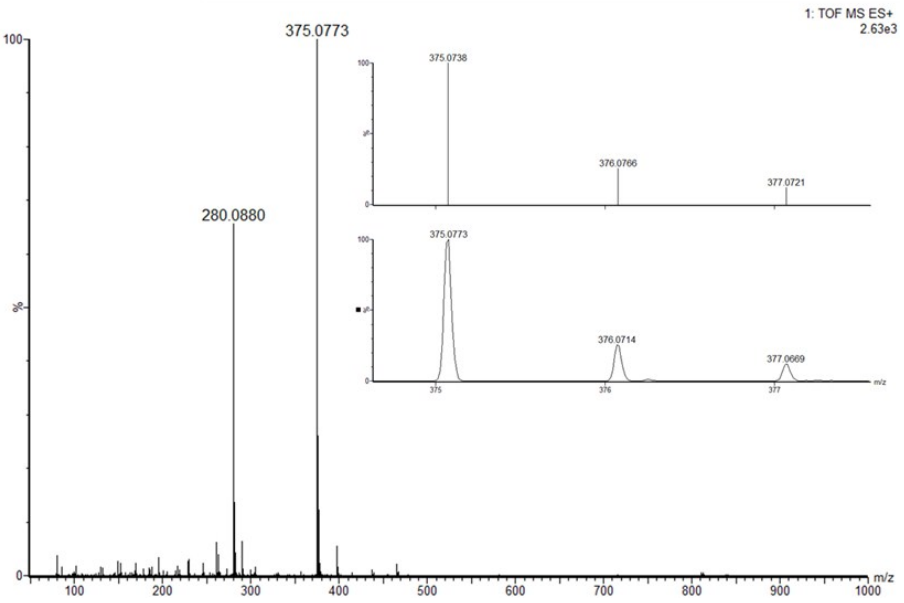

Figure S2. High resolution ESI-Mass spectrum of $[L+H]^+$, inset: the isotope pattern (bottom) with the simulated distribution (top)

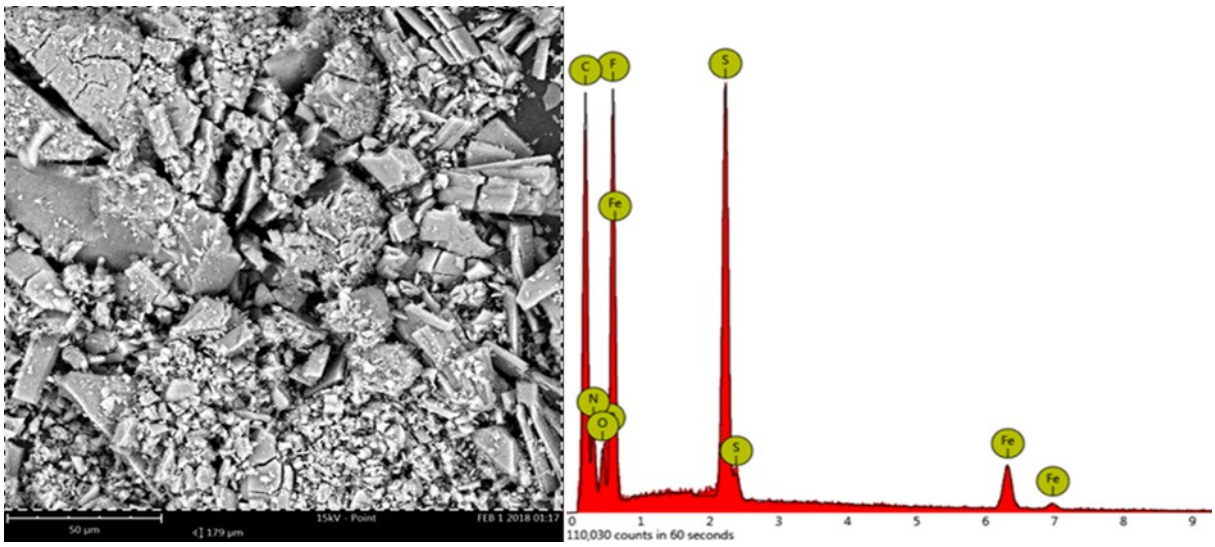

Figure S3: SEM image and SEM-EDS spectrum of cage **1**.

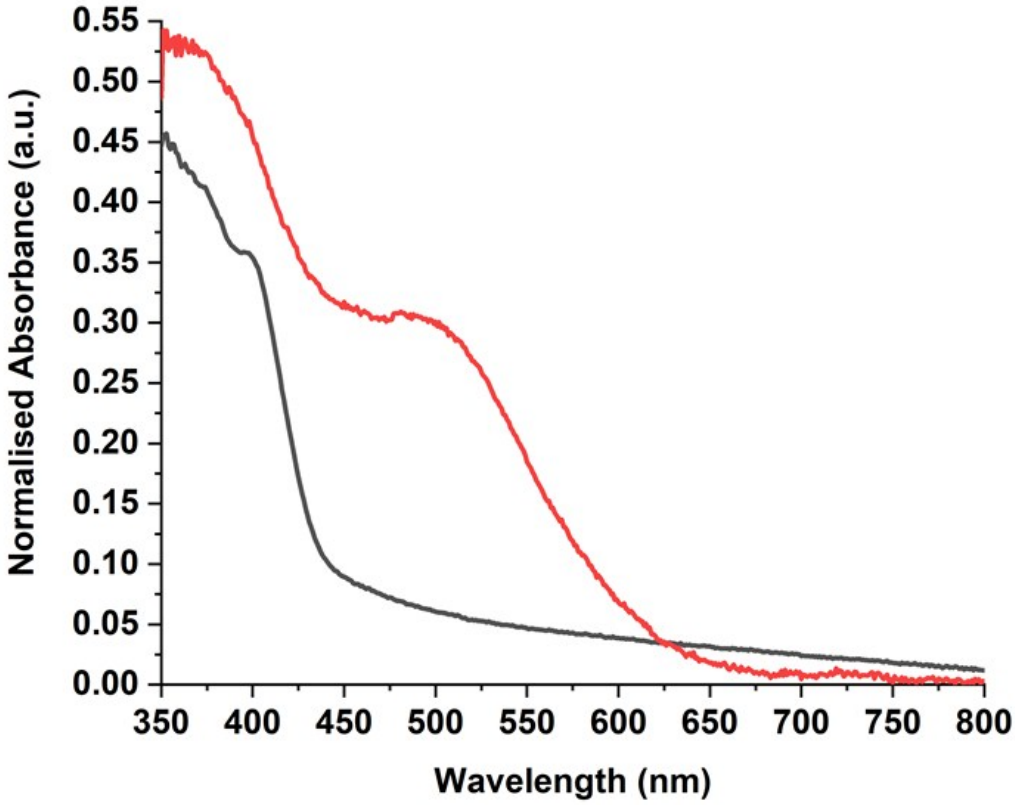

Figure S4: Solid-state Uv-Vis spectra of **L** (black) and **1** (red) in nujol.

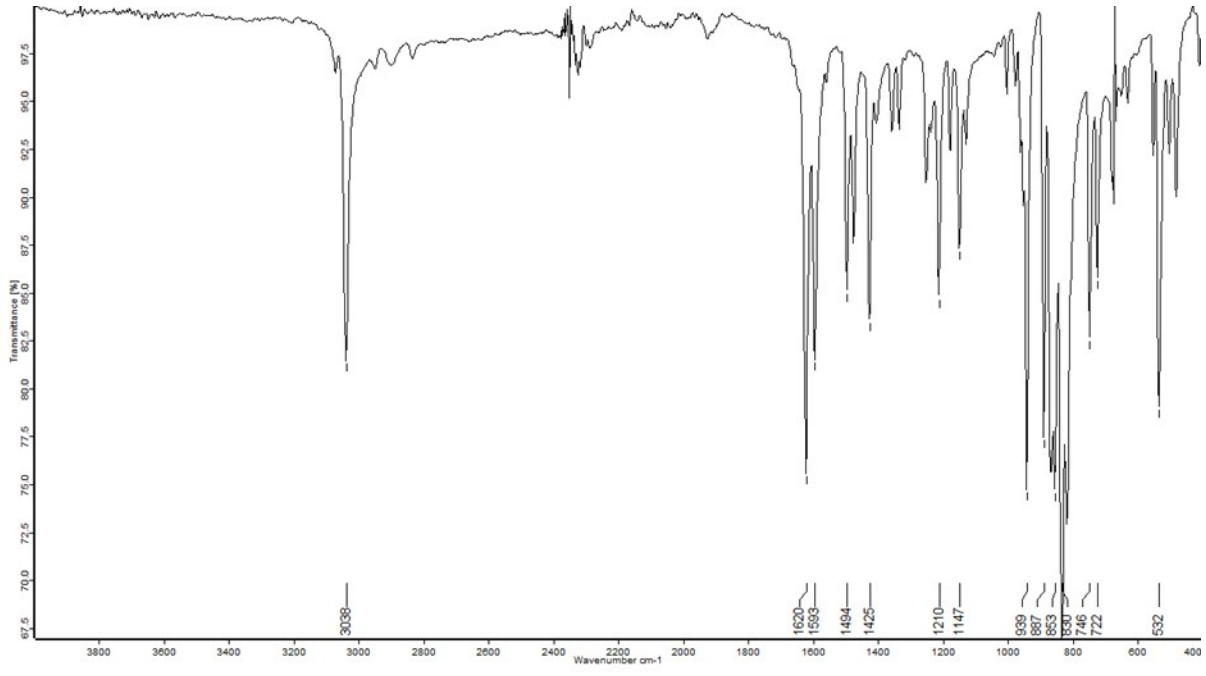

Figure S5: FT-IR spectra of **L**.

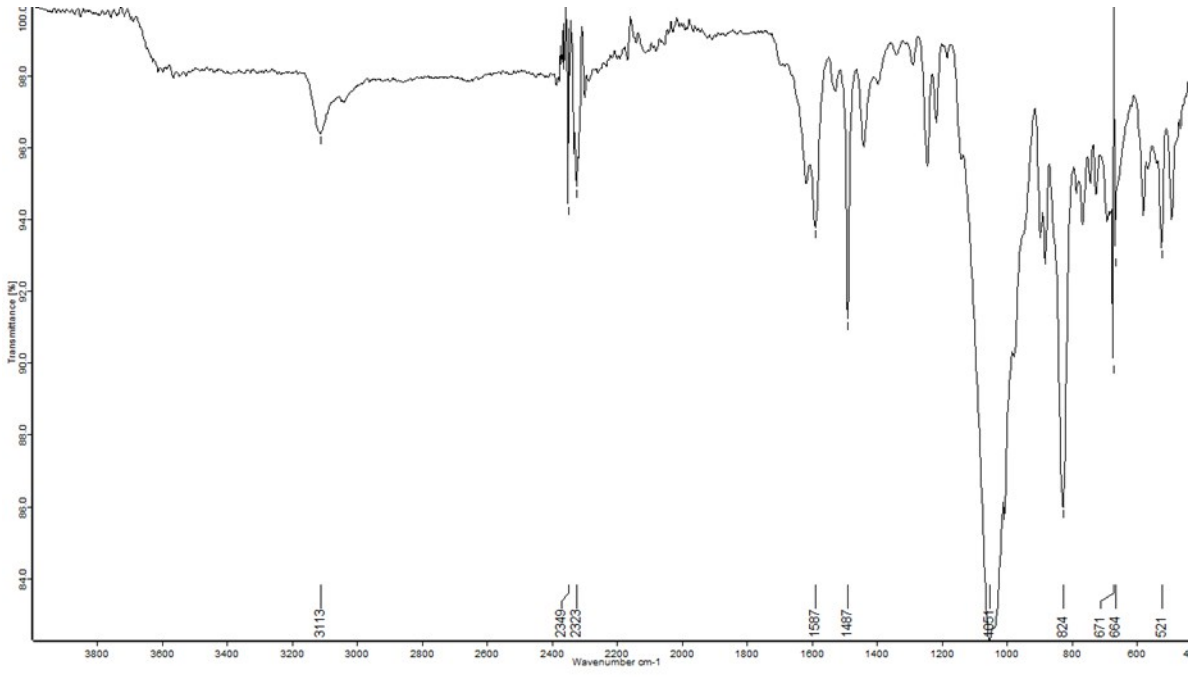

Figure S6: FT-IR spectra of **1**.

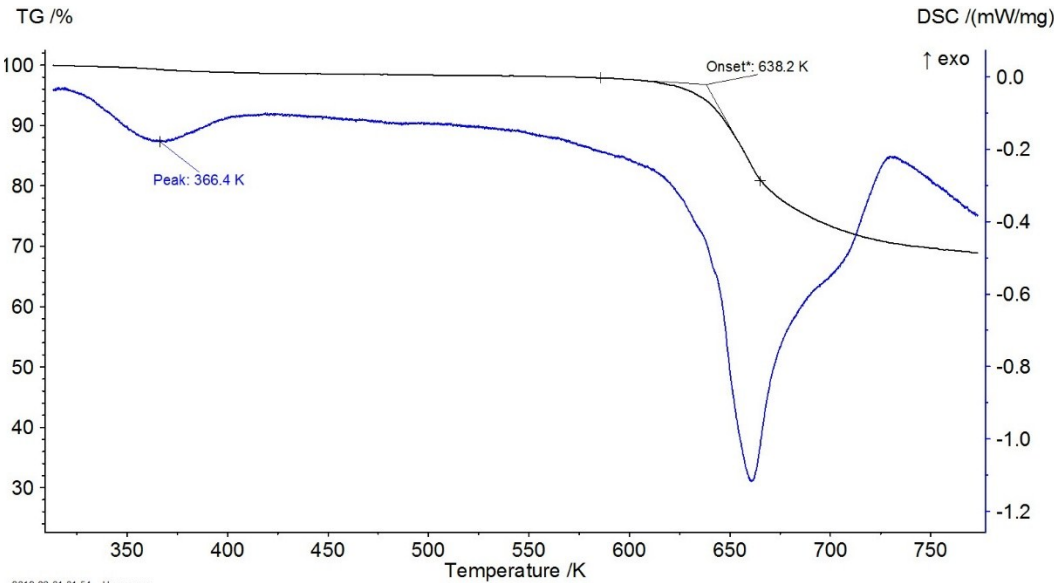

Figure S7: TGA and DSC spectra of **1** under argon gas measured from 300-770 K at 10 K per/min. Black line (TGA) and blue line (DSC).

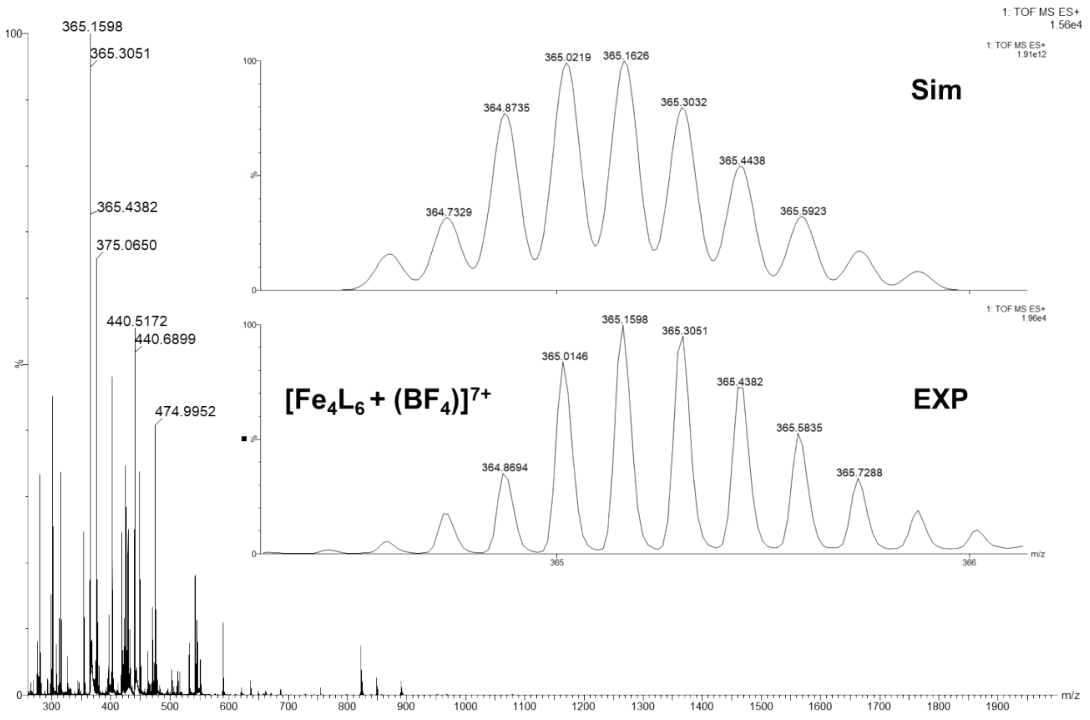

Figure S8 ESI-HRMS spectrum of **1**. The inset shows the isotope pattern for $[Fe_4\mathbf{L}_6 + (BF_4)]^{7+}$ with the simulated distribution.

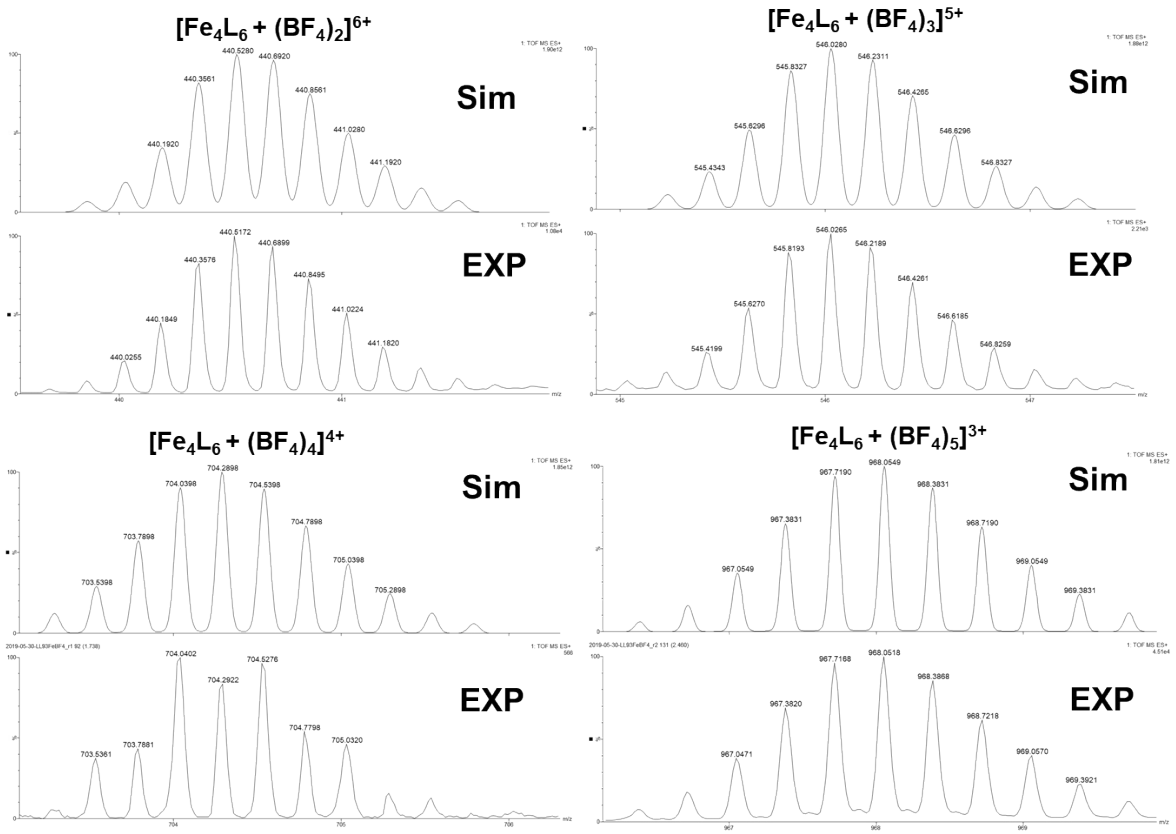

Figure S9 The isotope pattern for $[Fe_4\mathbf{L}_6 + (BF_4)_2]^{6+}$, $[Fe_4\mathbf{L}_6 + (BF_4)_3]^{5+}$, $[Fe_4\mathbf{L}_6 + (BF_4)_4]^{4+}$ and $[Fe_4\mathbf{L}_6 + (BF_4)_5]^{3+}$ with their simulated distribution, respectively.

Crystallography:

The single-crystal X-ray crystallography experiments were performed at the MX1 beamline of the Australian Synchrotron, using silicon double crystal monochromated radiation (0.7108 Å) at 100(2) K.[S2,3] Data integration and reduction were undertaken with XDS.[S4]. The structure was solved by intrinsic phasing using SHELXT [S5,] and the full-matrix least-squares refinements were carried out using SHELX[S6] via the OLEX-*2* graphical interface.[S7] Carbon-bound hydrogen atoms were included in idealised positions and refined using a riding model. Crystallographic data along with specific details pertaining to the refinement (inclusively addressing CheckCIF alerts), where required, follow. The crystallographic data in CIF format have been deposited at the Cambridge Crystallographic Data Centre with CCDC 1914986. It is available free of charge from the Cambridge Crystallographic Data Centre, 12 Union Road, Cambridge CB2 1 EZ, UK; fax: (+44) 1223-336-033; or e-mail: deposit@ccdc.cam.ac.uk.

The crystals rapidly lost solvent after removal from the mother liquor. Rapid (<1 min) handling at dry ice temperatures prior to quenching in the cryostream was required to collect data and multiple datasets from different crystals were merged. Despite these no reflection data was observed at better than 1.2 Å resolution. Nevertheless, the data is of more than sufficient quality to unambiguously establish the connectivity of the structure. Only heavy atoms (Fe, S) and the

encapsulated anions were refined anisotropically. Many of the other parts of the structure including the anions and solvent required bond length constraints and rigid body restraints to facilitate realistic modelling. In addition, reflecting the instability of the crystals, there is a large area of smeared electron density present in the lattice. Despite many attempts to model this region of disorder as a combination of solvent and anion molecules no reasonable fit could be found and accordingly this region was treated with the solvent masking procedure of OLEX-2,[S8] the 1200 electrons treated by this procedure correspond to the missing anion and approximately 12.5 acetonitrile solvent molecules per asymmetric unit.

Crystallographic data: $C_{138.5}H_{111.75}B_8F_{32}Fe_4N_{32}S_{12}$ (M =7183.57 g/mol): monoclinic, space group $P2_1/c$ (no. 14), a = 34.200(7) Å, b = 29.750(6) Å, c = 30.060(6) Å, β = 94.50(3)°, V = 30490(11) Å^3, Z = 8, T = 100(2) K, μ(Synchrotron) = 0.638 mm^{-1}, *Dcalc* = 1.537g/cm^3, 135734 reflections measured (1.194° ≤ 2Θ ≤ 34.454°), 18459 unique (R_{int} = 0.2661, R_{sigma} = 0.1245) which were used in all calculations. The final R_1 was 0.1110 (I > 2σ(I)) and wR_2 was 0.3240 (all data).

Table 1. Highlighted crystallographic parameters for **1**.

	Fe(II) centre	Average Fe-N bond length (Å)	∑ (°)	Spin-state	Average Intramolecular Fe···Fe distance (Å)	Volume of internal cavity (Å^3)
Cage A	Fe01	2.071	63.673	LS	12.738	206.88
	Fe02	1.962	77.379	LS		
	Fe03	1.973	65.347	LS		
	Fe04	2.207	114.163	HS		
Cage B	Fe05	2.059	68.182	LS	12.749	208.91
	Fe06	1.929	53.683	LS		
	Fe07	1.967	61.953	LS		
	Fe08	2.200	96.38	HS		

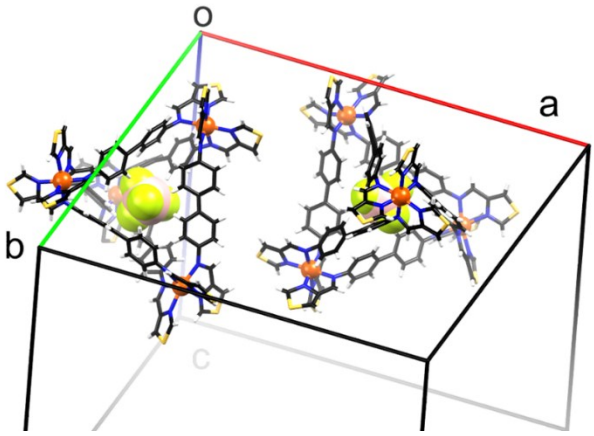

Figure S10. Schematic representation of the asymmetric unit of **1**, showing the two homochiral tetrahedral cages, A (right) **Δ, Δ, Δ, Δ** and B (left) **Λ, Λ, Λ, Λ** present in the asymmetric unit at 100 K with the encapsulated BF_4^- anions shown in a space-filling representation. Both structures are present in the [LS-LS-LS-HS] spin-state configuration at 100 K.

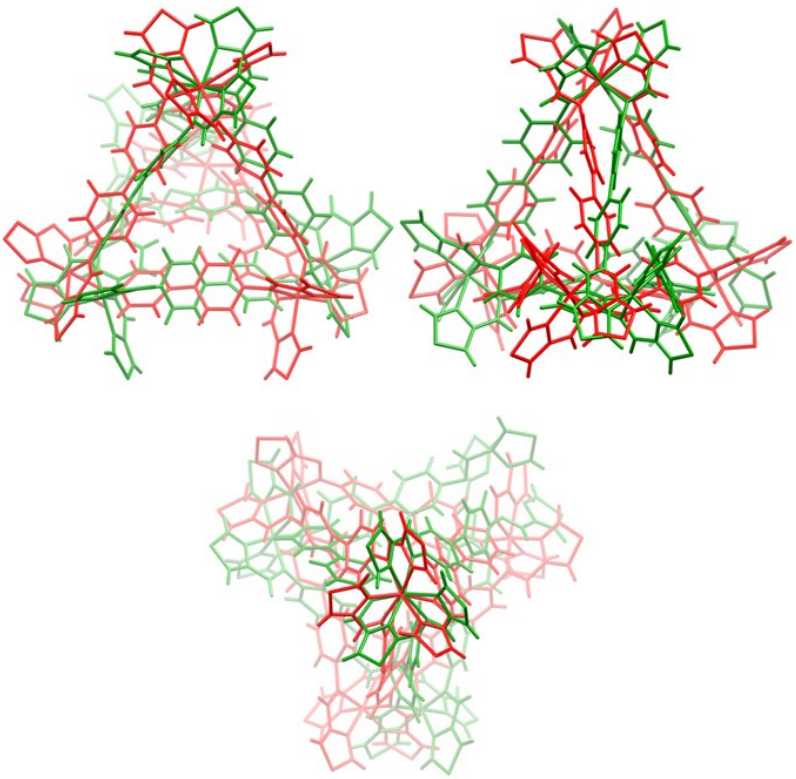

Figure S11. Molecular overlay of cage **A** and **B**, demonstrating the opposite chirality of the four Fe(II) centres in the respective tetrahedra (**A** = green - **Δ, Δ, Δ, Δ** and **B** = red - **Λ, Λ, Λ, Λ**) in the different directions.

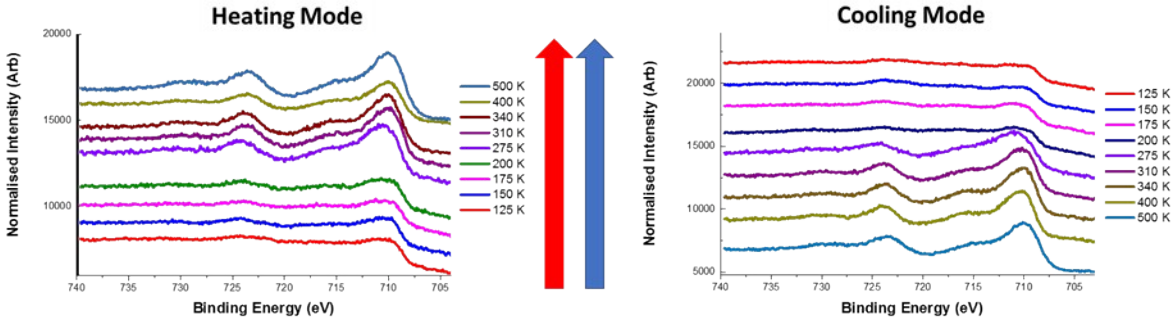

Figure S12: Cascade plot of VT-XPS experiments for **1**. The left-hand side corresponds to the heating mode, while the right-hand side corresponds to the cooling mode.

Method for relative HS fraction determination:

In order to obtain a HS fraction (%HS) the variable temperature XPS data was processed by optimising an offset and ratio of a mixture of the Fe 2p spectra measured at 100K and 400K to fit spectra measured at 125, 150, 175, 200, 275, 310, and 340K. The resulting spectral ratios were normalised and calibrated by setting the 100K XPS measurement to 25%HS and minimising the difference of the remaining values to the SQUID data. The sigmoidal function (%HS = c/(1.0+exp(-bt+a)), t=temp, a = 2.859, b = 0.006, c = 200), was fitted to the SQUID data.

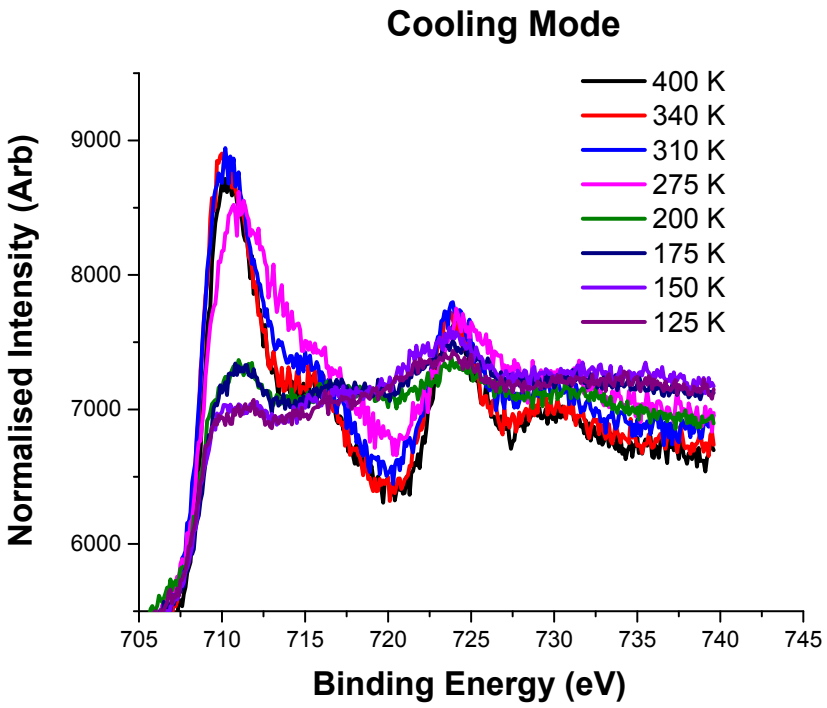

Figure S13. Temperature evolution of the Fe2p region in the X-ray photoelectron spectra of **1** in the cooling mode.

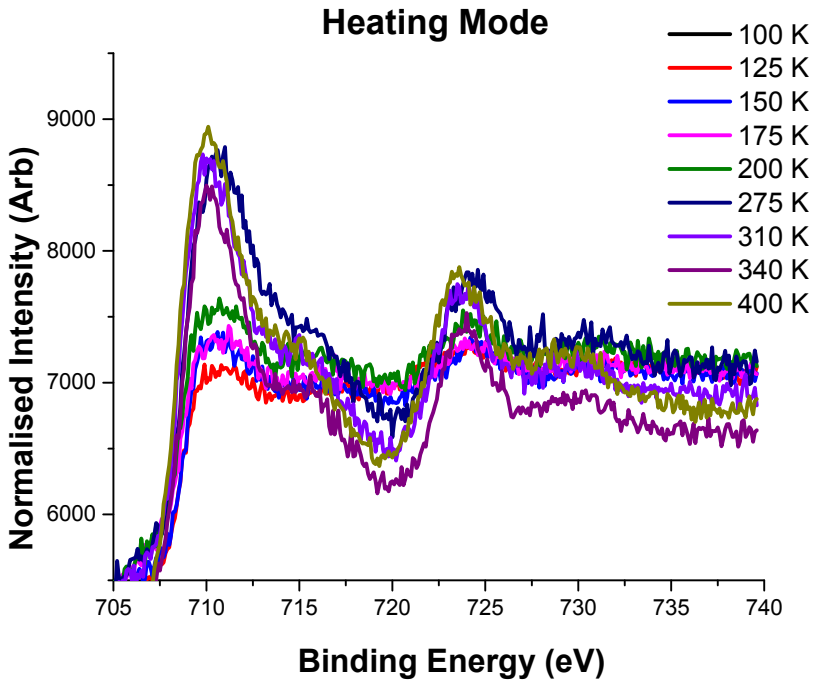

Figure S14. Temperature evolution of the Fe2p region in the X-ray photoelectron spectra of **1** in the heating mode.

References:

S1 J. K Clegg, J. Cremers, A. J. Hogben, B. Breiner, M. M. J. Smulders, J. D Thoburn,. and J. R. Nitschke, *Chem. Sci.* 2013, 68-76.

S2 N. P. Cowieson, D. Aragao, M. Clift, D. J. Ericsson, C. Gee, S. J. Harrop, N. Mudie, S. Panjikar, J. R. Price, A. Riboldi-Tunnicliffe, R. Williamson and T. Caradoc-Davies, *Journal of Synchrotron Radiation*, 2015, **22**, 187–190.

S3 T. M. McPhillips, S. E. McPhillips, H. J. Chiu, A. E. Cohen, A. M. Deacon, P. J. Ellis, E. Garman, A. Gonzalex, N. K. Sauter, R. P. Phizackerley, S. M. Soltis and P. Kuhn, *Journal of Synchrotron Radiation*, 2002, **9**, 401–406.

S4 W. Kabsch, *Journal of Applied Crystallography*, 1993, **26**, 795–800.

S5 G. Sheldrick, *SHELX-2014: Programs for Crystal Structure Analysis*, University of Göttingen, Göttingen, 2014.

S6 G. M. Sheldrick, *Acta Cryst C,* 2015, **71**, 3–8.

S7 O. V. Dolomanov, L. J. Bourhis, R. J. Gildea, J. A. K. Howard and H. Puschmann, *J. Appl. Cryst.*, 2009, **42**, 339–341.